



**HAL**  
open science

## Detecting overmature forests with airborne laser scanning (ALS)

Marc Fuhr, Etienne Lalechère, Jean-Matthieu Monnet, Laurent Bergès

► **To cite this version:**

Marc Fuhr, Etienne Lalechère, Jean-Matthieu Monnet, Laurent Bergès. Detecting overmature forests with airborne laser scanning (ALS). *Remote Sensing in Ecology and Conservation*, 2022, 8 (5), pp.731-743. 10.1002/rse2.274 . hal-03749422

**HAL Id: hal-03749422**

**<https://hal.science/hal-03749422>**

Submitted on 27 Oct 2023


**HAL** is a multi-disciplinary open access archive for the deposit and dissemination of scientific research documents, whether they are published or not. The documents may come from teaching and research institutions in France or abroad, or from public or private research centers.

L'archive ouverte pluridisciplinaire **HAL**, est destinée au dépôt et à la diffusion de documents scientifiques de niveau recherche, publiés ou non, émanant des établissements d'enseignement et de recherche français ou étrangers, des laboratoires publics ou privés.



Distributed under a Creative Commons Attribution - NonCommercial 4.0 International License

## ORIGINAL RESEARCH

**Detecting overmature forests with airborne laser scanning (ALS)**Marc Fuhr<sup>1</sup> , Etienne Lalechère<sup>2</sup>, Jean-Matthieu Monnet<sup>1</sup> & Laurent Bergès<sup>1</sup><sup>1</sup>INRAE, UR LESSEM, 2 rue de la Papeterie, BP 76, 38 402, Saint Martin d'Hères cedex, France<sup>2</sup>Université de Picardie Jules Verne, UR EDYSAN (UMR CNRS-UPJV 7058), 1 rue des Louvels, 80037, Amiens Cedex, France**Keywords**

airborne laser scanning, forest biodiversity, LiDAR, overmature forests

**Correspondence**

Marc Fuhr, INRAE, UR LESSEM, 2 rue de la Papeterie, BP 76, 38 402 Saint Martin d'Hères cedex, France. Tel: +33 4 76 76 27 28; E-mail: marc.fuhr@inrae.fr

Editor: Mat Disney

Associate Editor: Rocío Hernandez-Clemente

Received: 4 November 2021; Revised: 18

March 2022; Accepted: 19 April 2022

doi: 10.1002/rse2.274

*Remote Sensing in Ecology and Conservation* 2022; **8** (5):731–743**Abstract**

Building a network of interconnected overmature forests is crucial for the conservation of biodiversity. Indeed, a multitude of plant and animal species depend on forest structural maturity attributes such as very large living trees and deadwood. LiDAR technology has proved to be powerful when assessing forest structural parameters, and it may be a promising way to identify existing overmature forest patches over large areas. We first built an index (IMAT) combining several forest structural maturity attributes in order to characterize the structural maturity of 660 field plots in the French northern Pre-Alps. We then selected or developed LiDAR metrics and applied them in a random forest model designed to predict the IMAT. Model performance was evaluated with the root mean square error of prediction obtained from a bootstrap cross-validation and a Spearman correlation coefficient calculated between observed and predicted IMAT. Predictors were ranked by importance based on the average increase in the squared out-of-bag error when the variable was randomly permuted. Despite a non-negligible RMSEP (0.85 for calibration and validation data combined and 1.26 for validation data alone), we obtained a high correlation (0.89) between the observed and predicted IMAT values, indicating an accurate ranking of the field plots. LiDAR metrics for height (maximum height and height heterogeneity) were among the most important metrics for predicting forest maturity, together with elevation, slope and, to a lesser extent, with metrics describing the distribution of echoes' intensities. Our framework makes it possible to reconstruct a forest maturity gradient and isolate maturity hot spots. Nevertheless, our approach could be considerably strengthened by taking into consideration site fertility, collecting other maturity attributes in the field or developing adapted LiDAR metrics. Including additional spectral or textural metrics from optical imagery might also improve the predictive capacity of the model.

**Introduction**

An overmature forest stand is in the latest stages of forest dynamics, from the end of the growing stage to the collapse stage; these stages are often by-passed in forests managed for wood production. Overmature forests include true old-growth forests (OGF) but also forests

that are rarely or no longer logged, especially in the context of a specific silvicultural regime, known as retention silviculture (Gustafson et al., 2013).

Overmature forests are characterized by the following structural characteristics, the so-called maturity attributes (Bauhus et al., 2009; Cateau et al., 2015; Janssen, 2016; Paillet et al., 2010):

- a floristic structure dominated by native species,
- a heterogeneous dendrometric structure (well-distributed variety of diameters and heights) and the presence of very-large-diameter trees, leading to a high total basal area,
- a large volume of standing and lying deadwood, with a high diversity among pieces of lying deadwood in terms of dimension and degradation stage,
- the presence of numerous dendro-microhabitats (cavities, cracks, detached bark, sporophores of saproxylic fungi, *etc.*),
- a relatively open canopy with a heterogeneous distribution in terms of gap size class or closure stage. Recent studies have pointed out that overmature forests provide a large set of ecosystem services including carbon sinks (Luysaert et al., 2008), attractivity for ecotourism (Gunes & Hans, 2007), protection from rockfalls (Fuhr et al., 2015) and biodiversity conservation (Paillet et al., 2010). Numerous studies have highlighted that a multitude of plant and animal species depend on the structural attributes of overmature forests (Paillet et al., 2010):
- the quantity and quality of available deadwood strongly influences the specific or functional diversity of saproxylic organisms such as saproxylic beetles or saproxylic fungi (Janssen et al., 2016; Janssen et al., 2017), bryophytes and lichens (Dittrich et al., 2014),
- very large living and dying trees provide shelter and food for many birds species—especially cavity-nesting species such as woodpeckers or small mountain owls (Bütler et al., 2004) and bat species (Bouvet et al., 2016),
- a diversity of gap sizes leads to a significant heterogeneity of light conditions at ground level and benefits the specific and functional diversity of several taxa. Forests take centuries, even millenniums, to reach a stage of overmaturity. Conversely, overmature forests can be destroyed or degraded very quickly, even though setting aside protected areas can help limit this destruction. In addition, if a patch of overmature forest is too small, its mere presence may not be sufficient to provide resources for certain species with minimum area requirements (Pe'er et al., 2014). Forest managers usually classify patches of overmature forests according to size, from individual trees or small groups of trees to islets (around 1 ha) and forest reserves (10 to  $\geq 1000$  ha; Lachat & Bütler, 2007). Most of the species depending on overmature forest attributes disperse slowly (Komonen & Müller, 2018); therefore, building and maintaining networks of interconnected overmature forest patches is crucial to their conservation (Svensson et al., 2020).

The first step in creating a network of overmature forests is to identify existing patches. Currently, this identification process relies on detailed field protocols with numerous structural indicators that provide information on biodiversity, naturalness and overmaturity, for example, the WWF Old-Growth Forest Protocol or the

Potential Biodiversity Index (Larrieu & Gonin, 2008; Rossi & Vallauri, 2013). These protocols are costly and time-consuming and have only been implemented over small areas, making them unhelpful for building an adequate network at the landscape scale.

Early work exploring the potential of remote sensing to identify old-growth forests appeared with the introduction of Landsat images (Cohen & Spies, 1992; Jiang et al., 2004; Sabol et al., 2002). They focused mostly on conifer forests and aimed at separating young or adult even-aged stands with a regular structure from irregularly-structured overmature or old-growth stands. Recently, Spracklen and Spracklen (2019) obtained promising results in Ukraine by discriminating irregular OGFs from regular forest types with Sentinel-2 satellite images and by combining spectral indices and textural features. However, to our knowledge, these approaches fail to separate adult and overmature stands in irregular management systems, where structural differences between the two categories are much less pronounced.

The use of LiDAR (light detection and ranging) technology to assess forest structure has increased during the last decades, thanks to its ability to characterize the 3D structure of vegetation. Airborne Laser Scanning (ALS) is an active remote sensing system where an aircraft emits laser pulses towards the ground. The pulses are reflected by the obstacles and the distance to the emitting device is calculated from the time elapsed between the transmission of the signal and the reception of its return (or echo). The aircraft is also equipped with a GNSS (Global Navigation Satellite System) receiver and an inertial control unit so it is possible to precisely calculate the 3D coordinates of each surface element that has reflected one of the laser pulses. The resulting point cloud is then classified to differentiate the “ground” points, used to generate a digital terrain model (DTM), from other points interacting mainly with forest vegetation.

Two types of metrics can be extracted to characterize forest structure from the LiDAR point cloud. First, point cloud metrics are summary statistics that describe the point cloud in a given area. These commonly include the quantiles of the distribution of point heights above the ground, mean and standard deviations of height, and echoes' intensity values. These metrics are related to the 3D structure of the forest canopy as seen by the laser scanner. They are routinely used to predict forest stand structural variables such as dominant height, mean diameter, basal area or standing volume (White et al., 2013). Predictive models can be calibrated by linking stand dendrometric variables measured on field plots with the point cloud metrics extracted for the corresponding areas. However, such metrics do not directly translate into overmature forest attributes and this limits their utility for forest managers.

The second type of metrics, object-oriented metrics, relies on the use of geometrical criteria to identify objects such as trees, gaps and edges in the point cloud. It is also possible to derive summary statistics from these objects to supplement a set of explanatory variables (Glad et al., 2020). However, object-oriented metrics, such as the number of detected trees of a certain height or the proportion of area covered by gaps, do not necessarily improve model predictive power (Marchi et al., 2018).

Airborne LiDAR has now been used for several years for mostly management-oriented forest inventories. Applications to other ecosystems services, e.g. protection from rockfalls (Monnet et al., 2017) or biodiversity mapping (Bouvier et al., 2017; Glad et al., 2020), have also been tested. Using LiDAR data to identify mature forests is a recent technique that has mainly focused on the detection of one specific maturity attribute: deadwood. The results highlight that identifying deadwood elements, whether standing or lying, requires high point density, e.g. more than 20 pts./m<sup>2</sup> (see Marchi et al. (2018) for a review). Moreover, even with high point density, lying deadwood remains difficult to detect because the canopy and the shrub cover prevent beam penetration and because rocks often create noise. Indeed, as mentioned by Marchi et al. (2018), studies have been mostly located in areas where tree mortality was high and deadwood abundant.

However, even if the developed methods are becoming more and more sophisticated and promising, they may not be operational in areas where forest dynamics are dominated by small- to medium-scale disturbances, as it is the case in most European mountain forests (Brang et al., 2006). Nevertheless, studies focusing on medium- to large size deadwood elements (diameter > 30 cm) have obtained promising results (Mücke et al., 2013; Wing et al., 2015; Yao et al., 2012).

The objective of our study was to build a model able to predict forest maturity in areas dominated by managed forests with the LiDAR data commonly used for forest inventories over large areas (from 3 to 30 pts./m<sup>2</sup>). We first build a maturity index (IMAT) to characterize forest maturity in those stands. The IMAT combines three maturity attributes that may not all be simultaneously present at the same site: the total basal area of very large living trees, the total basal area of large dead standing trees and the volume of large lying woody debris. The IMAT was computed for a network of 660 field plots that were recently included in LiDAR surveys in the Northern French Alps. We then selected LiDAR metrics that had proven useful in predicting individual maturity attributes in other studies. We make the hypothesis that a combination of these LiDAR metrics is operational to accurately predict the index of maturity.

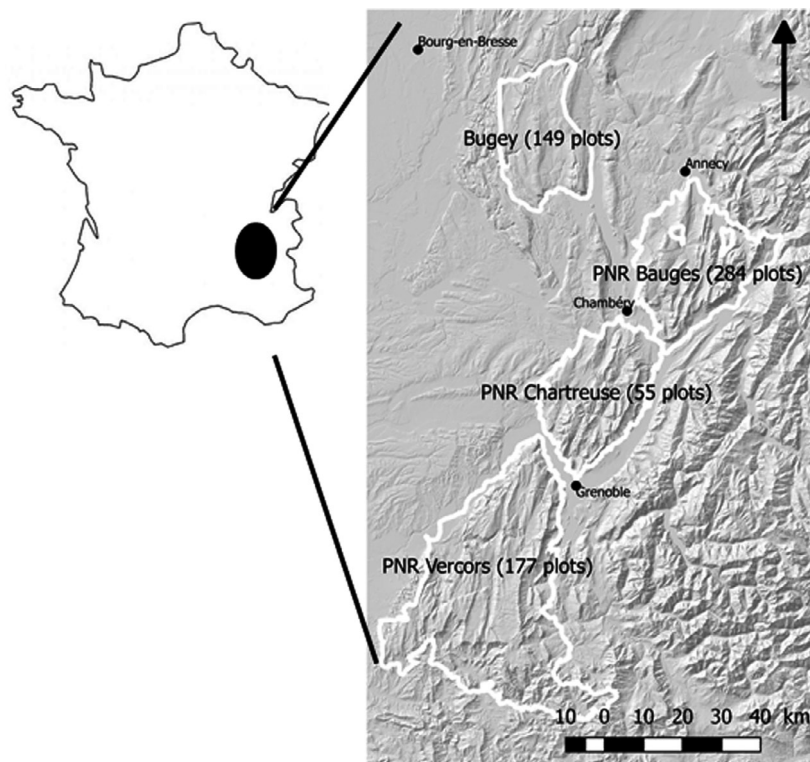


Figure 1. Location of the study sites.

## Materials and Methods

### Study sites and field data collection

The study area encompasses four mountain ranges in the French northern Pre-Alps: the Vercors, the Chartreuse, the Bauges and the Haut-Bugey (Fig. 1). These mountain ranges are quite similar in terms of substratum (limestone), climate (temperate) and altitude. The forest stands are pure or mixed dominated by European beech (*Fagus sylvatica*), silver fir (*Abies alba*) and, in places, Norway spruce (*Picea abies*). The dominant silvicultural system favours uneven-aged stands through single-tree or small-group selection cutting. Due to accessibility constraints, the lack of logging roads, natural hazard protection zones and ownership division, intensive management has hitherto been quite low, allowing overmature forests to develop in places.

We assessed forest structural maturity in 660 field plots (Table 1) at elevations ranging from 634 m to 1745 m. Plots originated from diverse research projects that combine systematic sampling on selected sites and random sampling at the mountain range scale. Most of the plots (487) were set up between 2012 and 2018. We also included 173 plots set up between 2006 and 2010 in forest reserves that have not been managed at least over the last 50 years and where no major natural disturbance was recorded during the 2006–2018 period. The largest time difference between field data collection and ALS acquisition was 13 years (concerning 5 GNB plots in the Chartreuse mountain range). As the maturity index changes slowly in the absence of major disturbances, this time lag

is expected to bring noise in the data but obtained models are still relevant to map the distribution of the maturity index.

The field protocols differed slightly among plots but had several important points in common: they all have circular subplots with radii from 15 to 20 m whose centres were spatially located with a GNSS receiver and where very large living trees (diameter at breast height (dbh)  $\geq 77.5$  cm), large dead standing trees (dbh  $\geq 30$  cm) and large lying woody debris ( $\geq 30$  cm in diameter at the narrow end and  $\geq 0.5$  m in length) were recorded. Very large living trees and large snags were measured in dbh. The diameter of the large lying woody debris was measured at both ends and the length of each debris piece located inside the plot was recorded. All diameters were measured using a tree caliper. Some field protocols included additional measurements that were not considered to assess stand maturity.

### Assessing plot maturity

For each plot  $i$ , we built a maturity index combining three structural attributes with well-known links to maturity:

- the total basal area of very large living trees ( $G_{VLLT}$ ,  $m^2 \cdot ha^{-1}$ ),
- the total basal area of large dead standing trees ( $G_{LDST}$ ,  $m^2 \cdot ha^{-1}$ ),
- the volume of large lying woody debris ( $V_{LWD}$ ,  $m^3 \cdot ha^{-1}$ ). Three other important maturity attributes were not considered in the construction of the index:

**Table 1.** Plot measurement and LiDAR survey specifications.

Mountain range	Field Plot Dataset (Plot number, sampling design)*	Year of measurement	Flight period	LiDAR sensor	Mean point density ( $m^{-2}$ )
Chartreuse	GNB (10, R)	2006	Aug–Sept 2019	Riegl LMS Q680i	20
	PSDRF_Seuil (41, S)	2012			
	Janssen (4, R)	2014			
Vercors	GNB (9, R)	2006	Sept 2010 and Aug 2011	Riegl LMS Q560	14
	PSDRF_HP (164, S)	2007			
	Janssen (3, R)	2014			
Bauges	Grosso (41, S)	2012	Sept 2016 and Sept 2018	Riegl LMS Q780	5
	LPO (42, R)	2013		Riegl LMS Q780	24
	Fullie (54, S)	2013			
	Bellevaux (41, S)	2013			
	Clocher (9, S)	2013			
	Seythenex (1)	2013			
	Janssen (29, R)	2014			
Ain	Protest (63, S)	2018	Oct–Dec 2014	Riegl LMS Q680i	3
	PSDRF (58, S)	2015			
	Trameforet (91, R)	2018			

All the plots of PSDRF\_HP and half of the plots of GNB are located in forest reserves.

\*R: random, S: systematic.



- the stand floristic structure, since native species largely dominated our study sites,
- tree microhabitats, because most of our field datasets lacked reliable information for these attributes,
- the diversity of the degradation stages of the large lying deadwood debris because information was lacking for some plots.  $G_{VLLT}$ ,  $G_{LDST}$  and  $V_{LWD}$  values were capped at their respective 99% quantiles ( $\eta_{.99}$ ) to ensure that extreme values did not carry disproportionate weight in the subsequent calculations.

The maturity index ranges from 0 to 1 and was calculated as follows:

$$IMAT = \frac{1}{3} \left( \frac{G_{VLLT}}{\eta_{.99}(G_{VLLT})} + \frac{G_{LDST}}{\eta_{.99}(G_{LDST})} + \frac{V_{LWD}}{\eta_{.99}(V_{LWD})} \right).$$

We preferred to give each the same weight in a comprehensive approach considering that we lacked bibliographic references to assign a different weight to each attribute and that the dependence on maturity attributes varies among taxa.

### Selecting LiDAR metrics and topographical variables

LiDAR data were obtained from various ALS surveys whose specifications are given in Table 1. They were taken from 2010 to 2019, as most of the field data. Data pre-processing and classification were performed for each survey by the corresponding data providers. Ground points were separated from vegetation points with the TIN-iterative algorithm (Axelsson, 2000) to produce a digital terrain model (DTM). We used the *normalize\_height* function (tin algorithm option) implemented in *lidR* package (Roussel et al., 2020) to calculate the height of each vegetation point by subtracting the altitude value

from the ground elevation value interpolated at the planimetric coordinates. The desired LiDAR metrics were computed for the normalized point clouds extracted from discs whose centre points corresponded to the centres of the field plots. The discs had a horizontal radius of 35 m in order to include a buffer zone with a width that corresponded approximately to half of the average stand height (30 m). The LiDAR metrics were then either directly derived from the point cloud (heights and intensities of the vegetation returns) or calculated after the detection of individual trees. Calculations were performed with functions from the R package *lidaRtRee* version 3.1.2 (<https://cran.r-project.org/package=lidaRtRee>). The “tree\_segmentation” and “tree\_extraction” functions were applied for tree detection, on a 1-m resolution canopy height model derived from the LiDAR point cloud, with their defaults settings. The method relies on local maxima filtering algorithm (method 1 in Eysn et al., 2015). The performance of tree detection in ALS data depends on forest structure but dominant trees are usually well detected. We assume that tree-related metrics, which are summary statistics derived from the detected trees, will bring additional, interpretable information to the models even though detected trees are only an estimation of real ones. Point cloud metrics are computed using the function “aba\_metrics” with default parameters. This function relies on function “stdmetrics” from package *lidR* (version 3.2.3). An example is available at [https://gitlab.irstea.fr/jean-matthieu.monnet/lidartree\\_tutorials/-/wikis/Forest-structure-metrics-mapping](https://gitlab.irstea.fr/jean-matthieu.monnet/lidartree_tutorials/-/wikis/Forest-structure-metrics-mapping).

We then selected through a bibliographic synthesis a set of candidate predictor LiDAR metrics that had proved to be useful in previous studies (Table 2).

LiDAR metrics characterizing height distribution ( $Z_{max}$ ,  $Z_{mean}$ ,  $Tree_{meanH}$ ,  $Tree_{Sup30.density}$  and  $Z_{sd}$ ,  $Z_{kurt}$ ,  $Tree_{sdH}$ ,  $Tree_{giniH}$ ) may be good predictors for

**Table 2.** Candidate LiDAR metrics. The metrics in italics were computed from detected trees.

Metric type	Metric name	Metric definition
Maximum and mean heights	$Z_{max}$ , $Z_{mean}$	Maximum and mean height values of the points classified as vegetation in the point cloud (m)
	<i>Tree.meanH</i>	Mean height of detected trees (m)
Height distribution	<i>TreeSup30.density</i>	Density of detected trees above 30 m in height (stems.ha <sup>-1</sup> )
	$Z_{sd}$ , $Z_{kurt}$	Standard deviation and kurtosis of the height values of the points classified as vegetation in the point cloud
	<i>Tree.sdH</i> , <i>Tree.giniH</i>	Standard deviation and Gini coefficient of the heights of detected trees
Intensity	$I_{mean}$ , $I_{sd}$	Mean and standard deviations of the normalized intensities of the points classified as vegetation in the point cloud
Stand density	<i>Tree.density</i>	Density of detected trees (stems.ha <sup>-1</sup> )
Canopy cover	<i>Tree.canopy_cover</i>	Percentage of the plot area covered by the crowns of detected trees
Environmental variables	Elevation	Elevation above sea level (m)
	Slope	Slope (%)

very large trees. Similar metrics were found appropriate for predicting total stand basal area (Bright et al., 2013) and the density of large diameter trees (Korhonen et al., 2016). Indeed, even though beyond a certain diameter threshold, growth in diameter is no longer accompanied by growth in height, the largest trees are potentially also the highest (Jennings, 1999). Moreover, LiDAR metrics characterizing height distribution are also good predictors of large snags (Bater et al., 2009; Casas et al., 2016; Martinuzzi et al., 2009) or coarse woody debris volume (Pesonen et al., 2008).

In addition to height metrics, echoes' intensity information (Imean, Isd) provide information about the distribution of the photosynthetic and non-photosynthetic elements in the stand and are good predictors of total dead biomass (Kim et al., 2009b), snag basal area (Bright et al., 2013; Wing et al., 2015) and coarse woody debris volume (Pesonen et al., 2008). Kashani et al. (2015) pointed out that raw intensity values depend on acquisition geometry and LiDAR hardware. Due to missing information on the flight trajectory and the absence of overlap area between surveys, it was not possible to perform intensity correction, or intensity normalization based on histogram matching. However, to make intensity values comparable, values were standardized by survey using the mean and standard deviation of intensity values of points extracted in plots covered by the survey.

Moreover, assuming that the canopy of overmature stands may be slightly denser and more open than the surrounding stands, we selected a LiDAR metric related to tree density (Tree.density) and another one related to canopy cover (Tree.canopy\_cover). Casas et al. (2016) found that a similar metric, "fractional cover", was powerful for detecting snags. The selected LiDAR metrics were not highly correlated (Spearman correlation coefficient <0.85) except for the two metrics related to crown size (mean crown area and mean crown volume of detected trees), which thus were removed.

We added two topographical variables that may impact the spatial distribution of overmature forests: elevation and slope, which we considered appropriate proxies for logging accessibility.

## Statistical modelling and validation

We related the maturity index (IMAT) calculated from our field survey data to the selected LiDAR metrics and topographic variables with a random forest regression algorithm, a machine-learning technique based on multiple decision trees (Breiman, 2001). We assumed that between-predictor interactions are sufficient to translate data heterogeneity related to differences in point density

because a preliminary analysis showed that the addition of a variable related to LiDAR survey did not improve prediction accuracy. The random forests were grown with 1000 trees. The optimal value of the number of predictors sampled at each node of each tree was fixed to two according to a tuning procedure that minimized the out-of-bag error estimate (Liaw & Wiener, 2002). The predictive importance of each LiDAR metric was assessed through the average increase in the squared out-of-bag error when the variable was randomly permuted (Liaw & Wiener, 2002). Finally, the model was evaluated with two indices averaged over 100 replicates of a bootstrap cross-validation (70% and 30% partitioning for calibration and validation, respectively). First, we used the Root Mean Square Error of Prediction (RMSEP), which was divided by the mean observed IMAT to facilitate interpretation. Second, we computed the Spearman coefficient correlation between the observed and predicted maturity indices. We performed these analyses on the R software v.3.6.0 with the *randomForest* package v.4.6–14 (Liaw & Wiener, 2002). Third, we calculated three other validation indices following Gauch et al. (2003) who partitioned mean squared deviance into three independent additive components called squared bias (SB), nonunity slope (NU) and lack of correlation (LC). These three components are related to a comparison of observed and predicted values and quantify: a biased mean prediction and a rotation bias (considering the intercept or the slope of a linear regression line for SB or NU, respectively) and a lack of covariance (as measured by a Pearson coefficient correlation, LC).

## Results

### IMAT values

The capped values of the total basal area of very large living trees ( $G_{VLLT}$ ) and large standing dead trees ( $G_{LDST}$ ) ranged respectively from 0 to 15.7  $m^2 \cdot ha^{-1}$  (with an extreme value reaching 58.3  $m^2 \cdot ha^{-1}$ ) and 0 to 11.4  $m^2 \cdot ha^{-1}$  (with an extreme value reaching 25.4  $m^2 \cdot ha^{-1}$ ). The capped value of the volume of large lying woody debris ( $V_{LWD}$ ) ranged from 0 to 92  $m^3 \cdot ha^{-1}$  (with an extreme value reaching 284  $m^3 \cdot ha^{-1}$ ).

The three variables used to calculate the maturity index were not correlated (Fig. 2). In other words, the plots rich in very large trees were not necessarily rich in deadwood (lying or standing). Plots where the maturity index took a mean value can therefore be plots rich in very large trees (ageing stage) or plots rich in deadwood (senescence stage).

Most of the field plots were not mature: IMAT ranged from 0 to 1 with an average value of 0.14; more than half of the plots had an IMAT between 0 and 0.2.

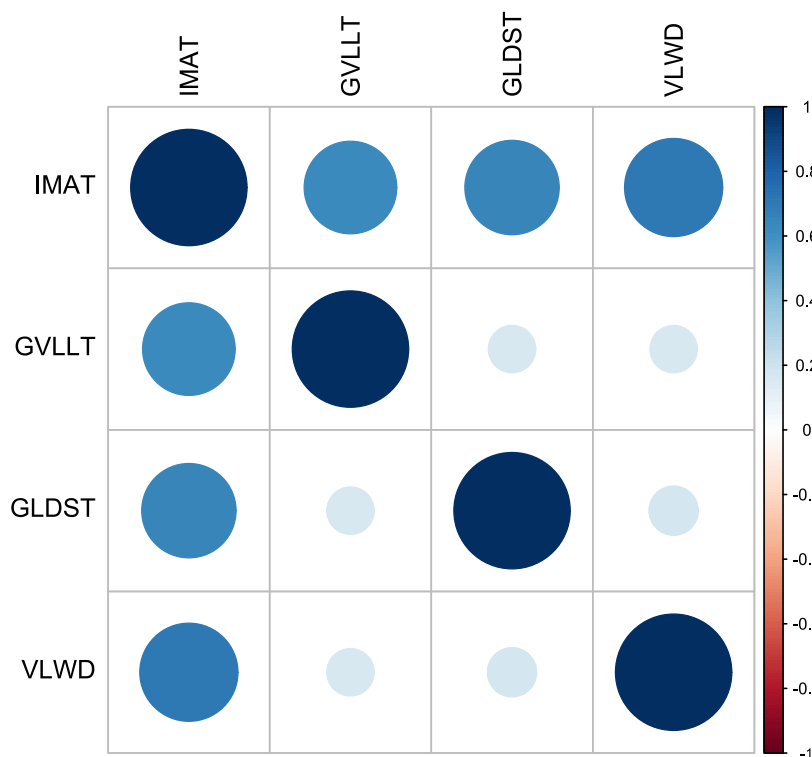


**Figure 2.** Correlations between maturity attributes within the field plot dataset.

**Model accuracy**

Mean estimation error was rather high, with a RMSEP of 0.85 for calibration and validation data combined and 1.26 for validation alone, when related to the mean IMAT value. This is explained by a prediction bias: low IMAT values tend to be slightly overestimated, while high values are underestimated by the model (Fig. 3). This result was confirmed by the partitioning of mean square deviance (NU = 0.002, LC = 0.0005, and SB = 0) that mainly come from a rotation bias (NU), little from a lack of correlation due to high error values (LC), and not from a biased mean prediction (SB). Finally, the rank correlation between observed and predicted values was high (Spearman correlation coefficient of 0.89). Prediction errors were not correlated with the difference of dates between LiDAR survey and plot field measurements.

**Predictor variable importance**

Elevation and slope ranked first in importance (Fig. 4); Zmax, Zmean, Zsd, Tree.density, Tree.meanH and TreeSup30.density were among the top eight predictive variables (Fig. 4); Isd and Tree.CanopyCover were of intermediate importance (Fig. 4); Zkurt, Tree.giniH, Tree.sdH and Imean were of quite low importance (Fig. 4).

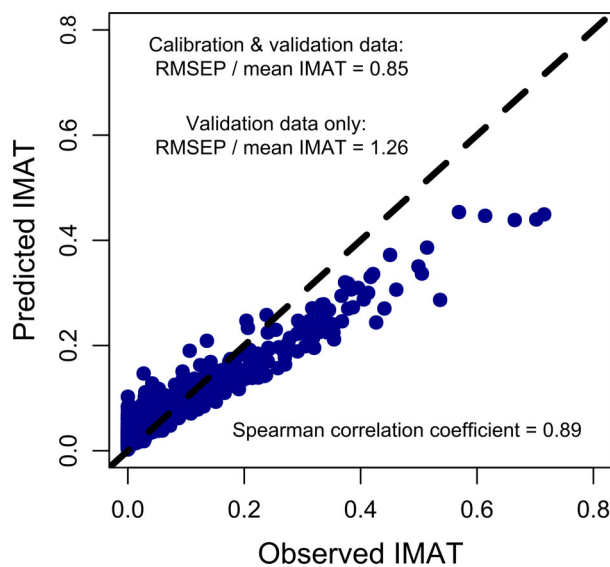


**Figure 3.** Relationship between observed and predicted maturity indices (IMAT). RMSEP: root mean square error of prediction. The dotted line is the 1:1 line (y = x).

**Predictor variable direction**

Forest maturity increased with the height metrics (Zmax, Zmean and TreeSup30.density), height distribution



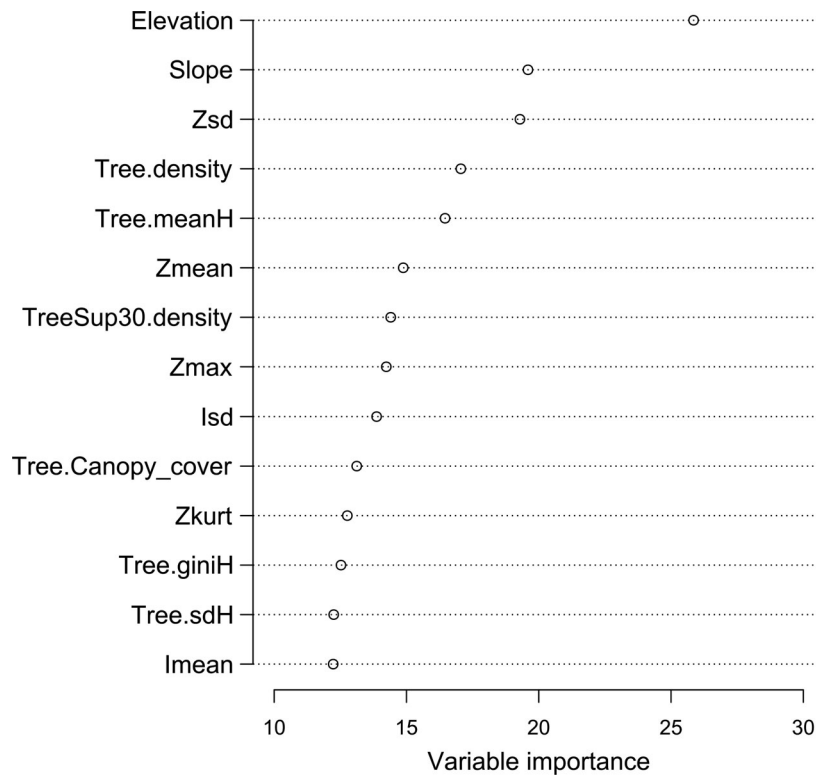


**Figure 4.** Importance of LiDAR metrics and topographical variables (average increase (in percent) in the squared out-of-bag error when the variable was randomly permuted) in predicting IMAT in the random forest model. See Table 2 for abbreviations.

heterogeneity (Zsd, Zkurt and Tree.sdH), intensity distribution heterogeneity (Isd) and mean intensity (lmean), even though the importance of lmean was rather low (Fig. 5). Forest maturity increased with slope and when elevation was above 1450 m a.s.l. (Fig. 5).

Forest maturity decreased strongly with tree density and increased slightly with canopy cover (Fig. 5).

Variations in forest maturity according to Tree.giniH (Fig. 5) did not show any clear trend. However, Tree.giniH had low predictive power.

## Discussion

Managers interested in mapping forest maturity for operational applications often have to rely on available field data and ALS surveys provided by public agencies. Cases where field and remote sensing data are not perfectly suited to this specific objective are likely to be common. Nevertheless, the results obtained in this study showed that modelling a maturity index is possible by combining several field and ALS datasets not specifically designed for this purpose.

Our results showed that the use of a combination of LiDAR metrics, that had proven useful in predicting

forest maturity attributes, is operational to predict the structural maturity of irregular forests dominated by beech and fir in the French pre-Alps, which validates our hypothesis.

Almost all the expected relationships between the maturity index and the LiDAR metrics were confirmed by our statistical model. Stand structural maturity was positively correlated with the LiDAR metrics quantifying (maximal?) height, height distribution heterogeneity, intensity distribution heterogeneity, and negatively correlated with the LiDAR metrics quantifying tree density and canopy cover.

The LiDAR metrics describing height (maximum and heterogeneity) were among the variables with the strongest ability to increase predictive accuracy. These results are consistent with other studies that have emphasized the importance of height distribution in predicting characteristic attributes of structural maturity: total stand basal area (Bright et al., 2013), density of large trees (Korhonen et al., 2016), tree diameter distributions (Bock et al., 2020), snag density or basal area (Bater et al., 2009; Casas et al., 2016; Martinuzzi et al., 2009) and lying deadwood volume (Pesonen et al., 2008).

The LiDAR metrics describing intensity distribution were also important predictors of forest maturity,

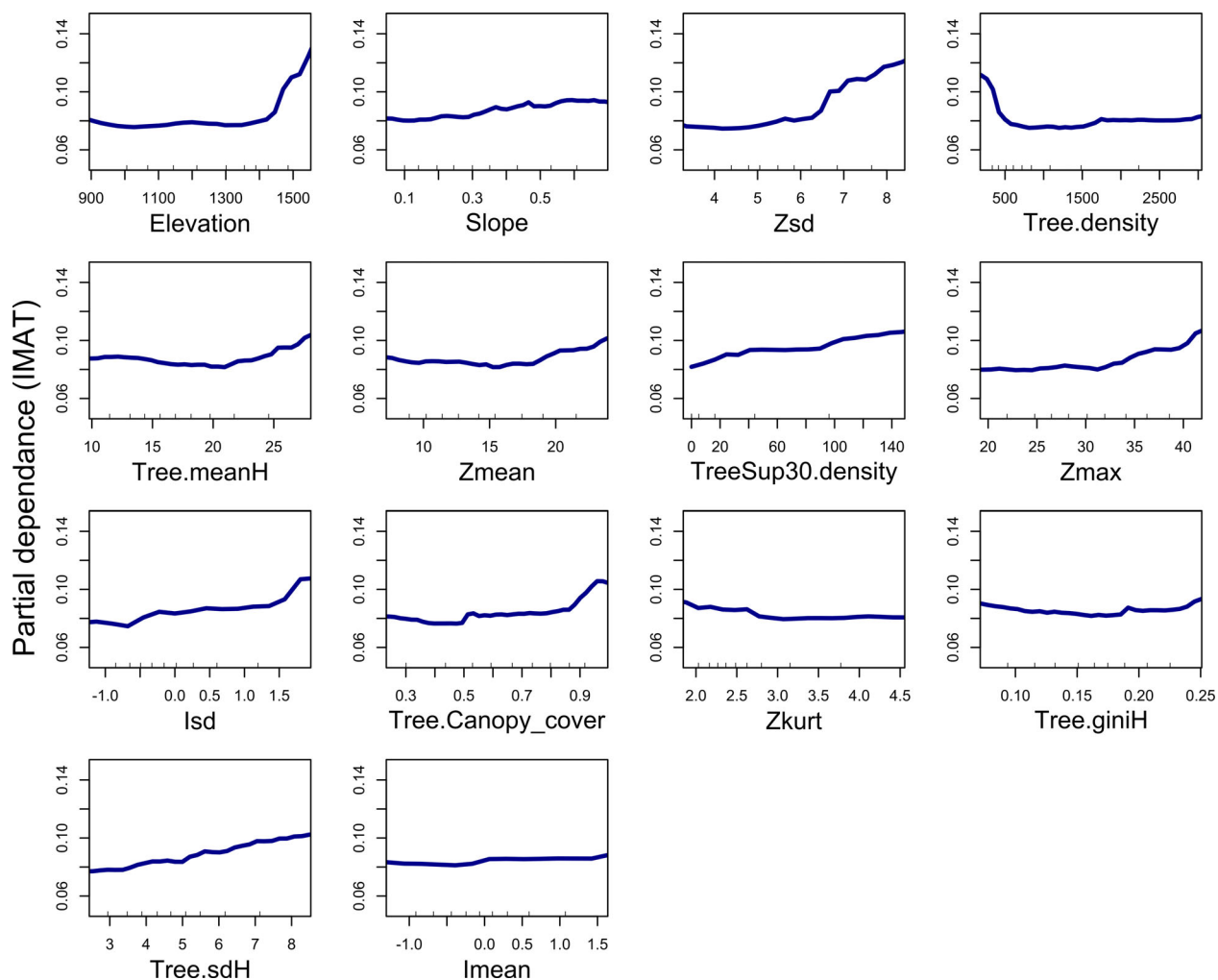


**Figure 5.** Relationship between the maturity index (IMAT) and LiDAR or topography variables. Partial dependence is the response of the maturity index on one predictor variable after averaging out the effects of the other predictor variables (Friedman, 2001).

although to a lesser extent. We centred and scaled the intensity distributions for each survey, but seasonal differences in data acquisition and different equipment settings among surveys might have induced some among-survey variability in intensity distribution (Kim et al., 2009a). That may explain why intensity-related metrics had such a low predictive power. However, our results confirm previous findings linking these metrics to the presence of standing or lying deadwood pieces (Bright et al., 2013; Kim et al., 2009b; Wing et al., 2015). Echo intensity depends on the varying photosynthetic capacity of living and non-living plant tissue, desiccated leaves or dead trees, for example. Improvement in intensity contribution to modelling might be possible if the variability due to acquisition and instruments can be reduced. As there is little convergence in intensity processing by data providers, technical options are left to end-users. Within-

survey variability due to acquisition geometry can be corrected if aircraft trajectory is available. Between-survey variability can be reduced by histogram matching in overlapping areas. If the field sample is large enough, one might consider building survey-specific models. An alternative to input radiometric information would be to use airborne or satellite imagery, which might provide more homogeneous data, more bands and possibly with a higher time frequency, at the expense of a lower resolution.

Contrary to our assumptions, IMAT was not positively correlated with the LiDAR metrics quantifying canopy openness or tree density. Overmature field plots in our dataset were mostly in the ageing stage of forest succession; the stands were dominated by very large trees that were quite distant from each other but whose crowns joined, leaving few gaps. In addition, as the irregular

silvicultural system favours the creation of small gaps, the canopy of adult stands may be more open than the canopy of overmature stands. Algorithms that detect trees from a 2D segmentation of the canopy height model are usually successful in detecting dominant and co-dominant trees, especially in coniferous stands (Eysn et al., 2015). However, the proportion of detections among suppressed trees is low and depends on forest structure. As a result, we can expect that density of tall detected trees (e.g. density of trees higher than 30 m) is close to what would be measured on the field. In contrast, the density of all detected trees is likely to be very different from its field counterpart, especially in young, homogeneous and broadleaved stands.

Finally, slope and elevation are two key environmental variables for predicting forest maturity. Logging difficulties increase with slope (Gauquelin & Courbaud, 2006) and the most mature stands are therefore often encountered on steep slopes.

The very good correlation between the observed and predicted IMAT values was nonetheless associated with non-negligible estimation errors, mainly due to a predictive bias. The partitioning of mean squared deviance indicated a very accurate average prediction and limited residual errors, when considered independently from the bias. However, our model underestimates the maturity of the most mature stands and slightly overestimates the maturity of the less mature ones. The underestimation of the maturity of the most mature stands probably partly

originates from the fact that, above a certain diameter, tree growth in diameter is no longer accompanied by growth in height (Jennings, 1999). The LiDAR metrics quantifying maximal height are therefore capped at a maximal value, even though tree diameters are still growing slightly. Probably for the same reason, other studies predicting tree diameters failed to predict very large trees (Bock et al., 2020).

Our approach relies on heterogeneous field datasets and LiDAR surveys point densities, parameters that may be sources of prediction errors potentially interacting. Further works of interest would be to test the sensibility of the model to each parameter. Nevertheless, our model can immediately be used to map forest maturity in areas covered by a LiDAR campaign (Fig. 6). Even though the maturity index should be interpreted with care considering the existing prediction errors, the least and most mature forest stands can be accurately identified by thresholding the maturity index. This meets the needs of many managers who are targeting conservation actions in natural areas or aim at constructing a connected ecological network of mature forest patches to preserve biodiversity for taxa depending on maturity attributes. De Assis Barros and Elkin (2021) recently suggested a similar approach for conifer forests in British Columbia. We believe that selecting a limited number of metrics which are easy for forest managers to understand is important in a management perspective. Once the areas to target for conservation measures, or other areas of interest, have

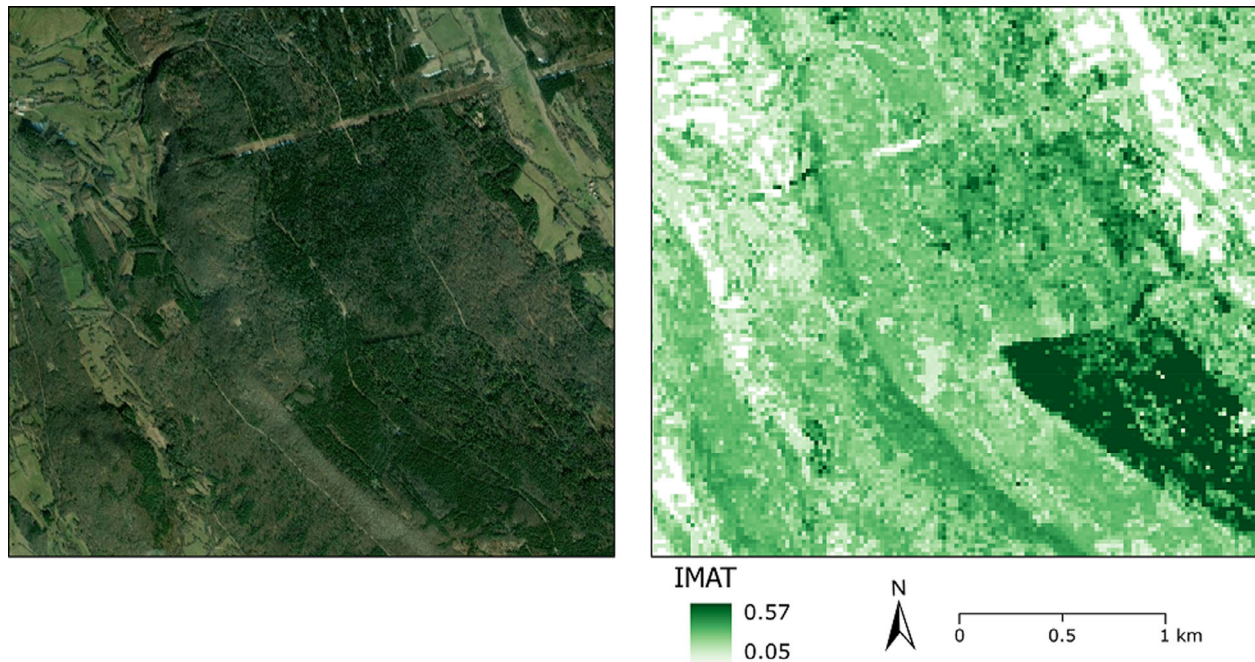


Figure 6. Local example of IMAT prediction in forests. The left panel represents an ortho-image. IMAT, maturity index.

been identified, it is then possible to investigate which metrics contribute to the maturity index and how. Taking the link between LiDAR metrics and forest structure into account may help managers to adopt specific silvicultural practices to improve the maturity of their forests.

Site fertility is very heterogeneous in the northern French Pre-Alps. When fertility is low (for example on very rocky or shallow soils), neither living nor dead trees can reach the same dimensions (diameter, height) as when fertility is high. Consequently, the diameter thresholds we used to calculate the maturity index in the field may not be suitable for some plots. In a study of overmature forests, Larrieu & Gonin (2008) suggest adapting the diameter threshold to 40 cm for living trees and to 20 cm for deadwood pieces in sites with very low fertility, as in some subalpine areas. In poor site conditions, LiDAR height metrics are capped at maximal local values even though these values could be intermediate at a broader scale. It may therefore be necessary to include additional environmental variables or LiDAR metrics linked to site fertility when building the prediction model. An option in irregular stands could consist in building and testing LiDAR metrics calibrated at a very local scale. As an example, the TreeSup30.density metric we used in our study could be replaced by a height metric representing the 95<sup>th</sup> percentile of the heights of the detected trees in a defined neighbourhood of the field plot.

Similarly, a stand's recent silvicultural history impacts its structural maturity. As an example, overmature copice stands may locally concentrate maturity attributes that are overlooked with the diameter thresholds we adopted (Lassauce et al., 2012). Here again, considering a silvicultural effect could modify both IMAT calculation and prediction. Recent methodological developments based on multi-sensors highlight the complementarity between LiDAR and optical data for forest structure modelling. LiDAR data have proven their ability to characterize 3D structures, while optical imagery can inform on species composition or health status. Spectral properties in the near-infrared region of the light spectrum or indices, like NDVI, based on combinations of reflectance in various bands, are useful to detect snags (Bütler & Schlaepfer, 2004; Zielewska-Büttner et al., 2020). Combining spectral and textural information from optical data with 3D information from LiDAR data or stereo photogrammetry will lead to more and more efficient models and more reliable cartographic information.

## References

Axelsson, P. (2000) DEM generation from laser scanner data using adaptative TIN models. *International Archives of the Photogrammetry, Remote Sensing*, **XXXIII**, 110–117.

- Bater, C.W., Coops, N.C., Gergel, S.E., LeMay, V. & Collins, D. (2009) Estimation of standing dead tree class distributions in northwest coastal forests using lidar remote sensing. *Canadian Journal of Forest Research*, **39**, 1080–1091. <https://doi.org/10.1139/X09-030>
- Bauhus, J., Puettmann, K. & Messier, C. (2009) Silviculture for old-growth attributes. *Forest Ecology and Management*, **258**, 525–537. <https://doi.org/10.1016/j.foreco.2009.01.053>
- Bock, J., Munoz, A., Riond, C., Monnet, J.-M. & Fuhr, M. (2020) *Chaîne de traitement pour la production de cartes forestières à partir de données LiDAR ou photogrammétriques, Rapport de synthèse PSDR4*. Chambéry, France: IOOffice National des Forêts, IRSTEA.
- Bouvet, A., Paillet, Y., Archaux, F., Tillon, L., Denis, P., Gilg, O. et al. (2016) Effects of forest structure, management and landscape on bird and bat communities. *Environmental Conservation*, **43**, 148–160. <https://doi.org/10.1017/S0376892915000363>
- Bouvier, M., Durrieu, S., Gosselin, F. & Herpigny, B. (2017) Use of airborne lidar data to improve plant species richness and diversity monitoring in lowland and mountain forests. *PLoS One*, **12**, e0184524. <https://doi.org/10.1371/journal.pone.0184524>
- Brang, P., Schönenberger, W., Frehner, M., Schwitter, R. & Wasser, B. (2006) Management of protection forests in the European Alps: an overview. *Forest Snow and Landscape Research*, **80**, 23–44.
- Breiman, L. (2001) Random forests. *Machine Learning*, 5–32.
- Bright, B.C., Hudak, A.T., McGaughey, R., Andersen, H.-E. & Negron, J. (2013) Predicting live and dead tree basal area of bark beetle affected forests from discrete-return lidar. *Canadian Journal of Remote Sensing*, **39**, 13.
- Bütler, R., Angelstam, P., Ekelund, P. & Schlaepfer, R. (2004) Dead wood threshold values for the three-toed woodpecker presence in boreal and sub-alpine forest. *Biological Conservation*, **119**, 305–318. <https://doi.org/10.1016/j.biocon.2003.11.014>
- Bütler, R. & Schlaepfer, R. (2004) Spruce snag quantification by coupling colour infrared aerial photos and a GIS. *Forest Ecology and Management*, **195**, 325–339. <https://doi.org/10.1016/j.foreco.2004.02.042>
- Casas, Á., García, M., Siegel, R.B., Koltunov, A., Ramírez, C. & Ustin, S. (2016) Burned forest characterization at single-tree level with airborne laser scanning for assessing wildlife habitat. *Remote Sensing of Environment*, **175**, 231–241. <https://doi.org/10.1016/j.rse.2015.12.044>
- Cateau, E., Larrieu, L., Vallauri, D., Savoie, J.-M., Touroult, J. & Brustel, H. (2015) Ancienneté et maturité: deux qualités complémentaires d'un écosystème forestier. *Comptes Rendus Biologies*, **338**, 58–73. <https://doi.org/10.1016/j.crvi.2014.10.004>
- Cohen, W.B. & Spies, T.A. (1992) Estimating structural attributes of Douglas-fir/western hemlock forest stands from



- landsat and SPOT imagery. *Remote Sensing of Environment*, **41**, 1–17. [https://doi.org/10.1016/0034-4257\(92\)90056-P](https://doi.org/10.1016/0034-4257(92)90056-P)
- de Assis Barros, L. & Elkin, C. (2021) An index for tracking old-growth value in disturbance-prone forest landscapes. *Ecological Indicators*, **121**, 107175. <https://doi.org/10.1016/j.ecolind.2020.107175>
- Dittrich, S., Jacob, M., Bade, C., Leuschner, C. & Hauck, M. (2014) The significance of deadwood for total bryophyte, lichen, and vascular plant diversity in an old-growth spruce forest. *Plant Ecology*, **215**, 1123–1137. <https://doi.org/10.1007/s11258-014-0371-6>
- Eysn, L., Hollaus, M., Lindberg, E., Berger, F., Monnet, J.-M., Dalponte, M. et al. (2015) A benchmark of lidar-based single tree detection methods using heterogeneous Forest data from the alpine space. *Forests*, **6**, 1721–1747. <https://doi.org/10.3390/f6051721>
- Friedman, J.H. (2001) Greedy function approximation: a gradient boosting machine. *The Annals of Statistics*, **29**, 1189–1232. <https://doi.org/10.1214/aos/1013203451>
- Fuhr, M., Bourrier, F. & Cordonnier, T. (2015) Protection against rockfall along a maturity gradient in mountain forests. *Forest Ecology and Management*, **354**, 224–231. <https://doi.org/10.1016/j.foreco.2015.06.012>
- Gauch, H.G., Hwang, J.T.G. & Fick, G.W. (2003) Model evaluation by comparison of model-based predictions and measured values. *Agronomy Journal*, **95**, 1442–1446. <https://doi.org/10.2134/agronj2003.1442>
- Gauquelin, X., Courbaud, B., 2006. Guide des sylvicultures de Montagne - Alpes du Nord françaises, CEMAGREF, ONF, CRPF Rhône-Alpes. ed.
- Glad, A., Reineking, B., Montadert, M., Depraz, A. & Monnet, J.-M. (2020) Assessing the performance of object-oriented LiDAR predictors for forest bird habitat suitability modeling. *Remote Sensing in Ecology and Conservation*, **6**, 5–19. <https://doi.org/10.1002/rse2.117>
- Gunes, G. & Hans, L. (2007) Ecotourism in old-growth forests in Turkey: the Kure Mountains experience. *Mountain Research and Development*, **27**, 281–283.
- Gustafson, L., bauhus, J., Kouki, J., Löhmus, A. & Sverdrup-Thygeson, A. (2013) Retention forestry - an integrated approach in practical use. In: Kraus, D. & Krumm, F. (Eds.) *Integrative approaches as an opportunity for the conservation of Forest biodiversity*, European Forest Institute, pp. 74–81.
- Janssen, P. (2016) *Influences relatives de l'ancienneté et de la maturité sur la biodiversité : implications pour la conservation en forêts de montagne*. PhD Thesis. Grenoble: Grenoble Alpes University.
- Janssen, P., Cateau, E., Fuhr, M., Nusillard, B., Brustel, H. & Bouget, C. (2016) Are biodiversity patterns of saproxylic beetles shaped by habitat limitation or dispersal limitation? A case study in unfragmented montane forests. *Biodiversity and Conservation*, **25**, 1167–1185. <https://doi.org/10.1007/s10531-016-1116-8>
- Janssen, P., Fuhr, M., Cateau, E., Nusillard, B. & Bouget, C. (2017) Forest continuity acts congruently with stand maturity in structuring the functional composition of saproxylic beetles. *Biological Conservation*, **205**, 1–10. <https://doi.org/10.1016/j.biocon.2016.11.021>
- Jennings, S. (1999) Assessing forest canopies and understorey illumination: canopy closure, canopy cover and other measures. *Forestry*, **72**, 59–74. <https://doi.org/10.1093/forestry/72.1.59>
- Jiang, H., Strittholt, J.R., Frost, P.A. & Slosser, N.C. (2004) The classification of late seral forests in the Pacific northwest, USA using Landsat ETM+ imagery. *Remote Sensing of Environment*, **91**, 320–331. <https://doi.org/10.1016/j.rse.2004.03.016>
- Kashani, A., Olsen, M., Parrish, C. & Wilson, N. (2015) A review of LIDAR radiometric processing: from ad hoc intensity correction to rigorous radiometric calibration. *Sensors*, **15**, 28099–28128. <https://doi.org/10.3390/s151128099>
- Kim, S., McGaughey, R.J., Andersen, H.-E. & Schreuder, G. (2009a) Tree species differentiation using intensity data derived from leaf-on and leaf-off airborne laser scanner data. *Remote Sensing of Environment*, **113**, 1575–1586. <https://doi.org/10.1016/j.rse.2009.03.017>
- Kim, Y., Yang, Z., Cohen, W.B., Pflugmacher, D., Lauver, C.L. & Vankat, J.L. (2009b) Distinguishing between live and dead standing tree biomass on the north rim of grand canyon National Park, USA using small-footprint lidar data. *Remote Sensing of Environment*, **113**, 2499–2510. <https://doi.org/10.1016/j.rse.2009.07.010>
- Komonen, A. & Müller, J. (2018) Dispersal ecology of deadwood organisms and connectivity conservation. *Conservation Biology*, **32**, 535–545. <https://doi.org/10.1111/cobi.13087>
- Korhonen, L., Salas, C., Østgård, T., Lien, V., Gobakken, T. & Næsset, E. (2016) Predicting the occurrence of large-diameter trees using airborne laser scanning. *Canadian Journal of Forest Research*, **46**, 461–469. <https://doi.org/10.1139/cjfr-2015-0384>
- Lachat, T. & Bütler, R. (2007) *Gestion des vieux arbres et du bois mort. Ilots de sénescence, arbres-habitat et métapopulations saproxyliques*. Lausanne: EPFL WSL.
- Larrieu, L. & Gonin, P. (2008) L'indice de biodiversité potentielle (IBP): une méthode simple et rapide pour évaluer la biodiversité potentielle des peuplements forestiers. *Revue Forestière Française*. **LX**, 727–748. <https://doi.org/10.4267/2042/28373>
- Lassaue, A., Anselme, P., Lieutier, F. & Bouget, C. (2012) Coppice-with-standards with an overmature coppice component enhance saproxylic beetle biodiversity: a case study in French deciduous forests. *Forest Ecology and Management*, **266**, 273–285. <https://doi.org/10.1016/j.foreco.2011.11.016>



- Liaw, A. & Wiener, M. (2002) Classification and regression by randomForest. *R News*, **2**, 6.
- Luyssaert, S., Schulze, E.-D., Börner, A., Knohl, A., Hessenmöller, D., Law, B.E. et al. (2008) Old-growth forests as global carbon sinks. *Nature*, **455**, 213–215. <https://doi.org/10.1038/nature07276>
- Marchi, N., Pirotti, F. & Lingua, E. (2018) Airborne and terrestrial laser scanning data for the assessment of standing and lying deadwood: current situation and new perspectives. *Remote Sensing*, **10**, 1356. <https://doi.org/10.3390/rs10091356>
- Martinuzzi, S., Vierling, L.A., Gould, W.A., Falkowski, M.J., Evans, J.S., Hudak, A.T. et al. (2009) Mapping snags and understory shrubs for a LiDAR-based assessment of wildlife habitat suitability. *Remote Sensing of Environment*, **113**, 2533–2546. <https://doi.org/10.1016/j.rse.2009.07.002>
- Monnet, J.-M., Bourrier, F., Dupire, S. & Berger, F. (2017) Suitability of airborne laser scanning for the assessment of forest protection effect against rockfall. *Landslides*, **14**, 299–310. <https://doi.org/10.1007/s10346-016-0687-5>
- Mücke, W., Deák, B., Schroiff, A., Hollaus, M., Pfeifer, N., 2013. Detection of fallen trees in forested areas using small footprint airborne laser scanning data. *Canadian Journal of Remote Sensing*, **10**.
- Paillet, Y., Bergès, L., Hjältén, J., Ódor, P., Avon, C., Bernhardt-Römermann, M. et al. (2010) Biodiversity differences between managed and unmanaged forests: meta-analysis of species richness in Europe. *Conservation Biology*, **24**, 101–112. <https://doi.org/10.1111/j.1523-1739.2009.01399.x>
- Pe'er, G., Tsianou, M.A., Franz, K.W., Matsinos, Y.G., Mazaris, A.D., Storch, D. et al. (2014) Toward better application of minimum area requirements in conservation planning. *Biological Conservation*, **170**, 92–102. <https://doi.org/10.1016/j.biocon.2013.12.011>
- Pesonen, A., Maltamo, M., Eerikäinen, K. & Packalèn, P. (2008) Airborne laser scanning-based prediction of coarse woody debris volumes in a conservation area. *Forest Ecology and Management*, **255**, 3288–3296. <https://doi.org/10.1016/j.foreco.2008.02.017>
- Rossi, M., Vallauri, D., 2013. Evaluer la naturalité. Guide pratique version 1.2, , WWF, Marseille. ed. WWF.
- Roussel, J.-R., Auty, D., Coops, N.C., Tompalski, P., Goodbody, T.R.H., Meador, A.S. et al. (2020) lidR: an R package for analysis of airborne laser scanning (ALS) data. *Remote Sensing of Environment*, **251**, 112061. <https://doi.org/10.1016/j.rse.2020.112061>
- Sabol, D.E., Gillespie, A.R., Adams, J.B., Smith, M.O. & Tucker, C.J. (2002) Structural stage in Pacific northwest forests estimated using simple mixing models of multispectral images. *Remote Sensing of Environment*, **80**, 1–16. [https://doi.org/10.1016/S0034-4257\(01\)00245-0](https://doi.org/10.1016/S0034-4257(01)00245-0)
- Spracklen, B.D. & Spracklen, D.V. (2019) Identifying European old-growth forests using remote sensing: a study in the Ukrainian Carpathians. *Forests*, **10**, 127. <https://doi.org/10.3390/f10020127>
- Svensson, J., Bubnicki, J.W., Jonsson, B.G., Andersson, J. & Mikusiński, G. (2020) Conservation significance of intact forest landscapes in the Scandinavian Mountains Green Belt. *Landscape Ecology*, **35**, 2113–2131. <https://doi.org/10.1007/s10980-020-01088-4>
- White, J.C., Wulder, M.A., Varhola, A., Vastaranta, M., Coops, N.C., Cook, B.D. et al. (2013) A best practices guide for generating forest inventory attributes from airborne laser scanning data using an area-based approach. Victoria, British Columbia: Canadian Forest Service.
- Wing, B.M., Ritchie, M.W., Boston, K., Cohen, W.B. & Olsen, M.J. (2015) Individual snag detection using neighborhood attribute filtered airborne lidar data. *Remote Sensing of Environment*, **163**, 165–179. <https://doi.org/10.1016/j.rse.2015.03.013>
- Yao, W., Krzystek, P. & Heurich, M. (2012) Identifying standing dead trees in forest areas based on 3D single tree detection from full waveform lidar data. *ISPRS Annals of the Photogrammetry, Remote Sensing and Spatial Information Sciences*, **1–7**, 359–364. <https://doi.org/10.5194/isprsannals-I-7-359-2012>
- Zielewska-Büttner, K., Adler, P., Kolbe, S., Beck, R., Ganter, L.M., Koch, B. et al. (2020) Detection of standing deadwood from aerial imagery products: two methods for addressing the bare ground misclassification issue. *Forests*, **11**, 801. <https://doi.org/10.3390/f11080801>